Imaging polyhedral inclusion bodies of nuclear polyhedrosis viruses with second harmonic generation microscopy

Tzu-Ming Liu[1], Yen-Wei Lee[1], Chieh-Feng Chang[1], Shih-Chia Yeh[2], Chung-Hsiung Wang[2], Shi-Wei Chu[3], and Chi-Kuang Sun[1,4*]

[1] Department of Electrical Engineering and Graduate Institute of Photonics and Optoelectronics, National Taiwan University, Taipei 10617, TAIWAN. R.O.C.
[2] Department of Entomology, National Taiwan University, Taipei 10617, TAIWAN. R.O.C.
[3] Department of Physics, National Taiwan University, Taipei 10617, TAIWAN. R.O.C.
[4] Research Center for Applied Sciences, Academia Sinica, Taipei 11529, TAIWAN. R.O.C.
*Corresponding author: sun@cc.ee.ntu.edu.tw

Abstract: We studied the polarization anisotropy of second harmonic generation (SHG) in polyhedral inclusion bodies (PIBs) of nuclear polyhedrosis viruses (NPV). Due to a body-centered-cubic arrangement of polyhedrin trimers, a characteristic SHG polarization property with a mixture of I23 and I3 symmetry was measured from PIBs. With this characteristic SHG anisotropy, it provides an intrinsic nonlinear signal for virus infection studies in living cells. With multimodal harmonic generation microscopy, we also demonstrated 3D imaging on PIBs of NPV in living cells. The distribution and the number of PIBs in intact infected cells can be revealed without the help of fluorescent labeling.

OCIS codes: (180.4315) Nonlinear microscopy; (190.4710) Optical nonlinearities in organic materials; (190.3970) Microparticle nonlinear optics

References and links

1. J. H. Chang, J. Y. Choi, B. R. Jin, J. Y. Roh, J. A. Olszewski, S. J. Seo, D. R. O'Reilly, Y. H. Je, "An improved baculovirus insecticide producing occlusion bodies that contain Bacillus thuringiensis insect toxin," J. Invertebr. Pathol. **84,** 30–37 (2003).
2. P. J. Harshman, T. K. Gustafson, and P. Kelley, "Baculovirus-mediated gene transfer into mammalian cells," Proc. Natl. Acad. Sci. *U.S.A.* **93**, 2348-2352 (1996).
3. T.-C. Lee, S.-M. Yu, and Y. C. Chao. "Fusion of foreign protein genes to the occlusion body gene of the baculovirus to assist protein isolation and antibody production," J. Genet. Mol. Biol. **16**, 138-150 (2005).
4. C.-K. Sun, S.-W. Chu, S.-Y. Chen, T.-H. Tsai, T.-M. Liu, C.-Y. Lin, H.-J. Tsai, "Higher harmonic generation microscopy for developmental biology," J. Struct. Biol. **147,** 19- 30 (2004).
5. Asian Vegetable Research and Development Center (AVRDC). AVRDC Annual Report 2004, W. Easdown and T. Kalb, eds., (AVRDC, Shanhua, Tainan, Taiwan, 2007).
6. S. C. Yeh, S. T. Lee, C Y. Wu, and C. H. Wang. "A cell line (NTU-MV) established from *Maruca vitrata* (Lepidoptera: pyralidae): characterization, viral susceptibility, and polyhdra production," J. Invertebr. Pathol. **96**, 138-146 (2007).
7. S.-Y. Chen, C.-S. Hsieh, S.-W. Chu, C.-Y. Lin, C.-Y. Ko, Y.-C. Chen, H.-J. Tsai, C.-H. Hu, and C.-K. Sun, "Noninvasive harmonics optical microscopy for long-term observation of embryonic nervous system development in vivo," J. Biomed. Opt. **11,** 054022 (2006).
8. R. M. Williams, W. R. Zipfel, and W. W. Webb, "Interpreting second-harmonic generation images of collagen I fibrils," Biophys. J. **88**, 1377-1386 (2005).
9. J.-X. Cheng and X. S. Xie, "Green's function formulation for third-harmonic generation microscopy," J. Opt. Soc. Am. B **19**, 1604-1610 (2002).
10. K. Anduleit, G. Sutton, J. M. Diprose, P. P. C. Mertens, J. M. Grimes, and D. I. Stuart, "Crystal lattice as biological phenotype for insect viruses," Protein Sci. **14**, 2741-2743 (2005).
11. F. Coulibaly, E. Chiu, K. Ikeda, S. Gutmann, P. W. Haebel, C. Schulze-Briese, H. Mori, and P. Metcalf, "The molecular organization of cypovirus polyhedra," Nature **446,** 97-101 (2007).
12. A. Yariv, *Optical Electronics in Modern Communications*, 5th ed. (Oxford University Press, 1997), pp. 330.

13. S.-W. Chu, S.-P. Tai, C.-K. Sun, and C.-H. Lin, "Selective imaging in second-harmonic-generation microscopy by polarization manipulation," Appl. Phys. Lett. **91,** 103903 (2007).

1. Introduction

In recent years, nucleopolyhedrovirus (NPV) has drawn a lot of attention due to its applications in biological pesticides [1], gene therapy [2], and production of foreign proteins. The NPV infected cells will express a large amount of polyhedrin to occlude reproductive virions into micrometer-sized polyhedral inclusion bodies (PIBs) in nuclei. When shielded by PIBs, NPV virions can remain infectious in harsh environment such as detergent or acid. Since the formation of PIBs is the final stage of viral infection, the rate and the yield of reproduction can thus be evaluated from the number of PIBs and from the time when they appear. These evaluations are useful diagnostic methods for studies of viral pathology and for mass production of pesticide or foreign proteins fused in PIBs [3]. Traditionally, the number of PIBs can be either counted with a hemocytometer or estimated from their optical density. However, these quantification methods require infected cells be lysed. Besides, in early stages of infection, the size of PIBs might be smaller than 1μm, making them difficult to be identified and counted under a conventional optical microscope. Here, for the first time, we demonstrated second harmonic generation (SHG) imaging on PIBs in infected cells. By rotating the polarization of incident laser pulses, the measured SHG intensities showed a periodical oscillation matching the crystal symmetry of the PIB crystal. Exploiting this characteristic polarization anisotropy of SHG signals and the 3D sectioning capability of multimodal harmonic generation microscopy [4], we successfully imaged the sizes and the 3D distribution of PIBs in living infected cells. The number of PIBs at a certain time after infection can thus be noninvasively evaluated in each cell without any stain.

2. Sample preparation and experimental setup

The virus used for this study, MaviMNPV (*M. vitrata* multiple nucleopolyhedrovirus), is a new NPV found in Taiwan [5]. MaviMNPV was propagated in its homologous cell line, NTU-MV cell line, established from pupal tissue of *Maruca vitrata* (MV) [6]. This cell line, cultured in a serum-free Sf900 medium, shows high susceptibility to MaviMNPV. After 3 days post-infection, nuclei of infected MV cells will expand to whole-cell sizes and some micrometer-sized PIBs can be identified with a traditional optical microscope by an experienced observer [6]. But some PIBs are smaller than 1 μm in size, which makes them hard to be distinguished from vesicles [6]. To image the presence and the distribution of PIBs in infected cells, we employed a laser-scanning higher-harmonic generation microscope (HGM) system [7]. It was adapted from an Olympus FV300 scanning unit combined with an Olympus BX51 upright microscope. The linearly-polarized light source was a home-built femtosecond Cr:forsterite laser, operating around 1230 nm with a repetition rate of 110 MHz and a pulse width of 140 fs. Real-time 2D scanning was achieved with a pair of high-speed galvanometer mirrors inside the scanning unit. The collimated laser beam was coupled into the scanning system connecting to an Olympus BX51 microscope with an aperture-fitting tube lens. Consequently, the laser beam was reflected by a mirror in BX51 and focused into infected cells through a 2-mm-working-distance high numerical-aperture (NA) infrared objective (LUMPlanF1/IR 60X/water/NA0.9, Olympus). The focused laser beam was scanned with a spot size close to its diffraction limit. The average power after the objective was 100 mW with a measured 100:1 contrast of polarization. Forward-generated SHG and third harmonic generation (THG) were collected by a high-NA condenser. The signals were guided into two photomultiplier tubes (PMT), which were synchronized with the galvanometer mirrors and used to record interference-filtered SHG and THG signals point by point to form 2D-sectioned images. The recording speed was 0.25–2.5 sec per frame, with 512×512 scanning points.

3. Multimodal harmonic generation microscopy of PIB

As a control, we first took multimodal harmonic generation microscopy images of the uninfected MV cells. No SHG signal was detected and only THG images of cells could be obtained. As shown in Fig. 1, due to the interface THG effect, we can clearly identify the membranes and organelles of living cells.
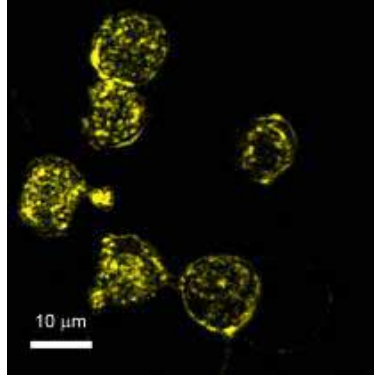

Fig. 1. Combined image of second harmonic generation (SHG) (green color) and third harmonic generation (THG) (yellow color) from uninfected cells in the NTU-MV cell line. No SHG can be found in uninfected cells.

Then we took multimodal harmonic generation microscopic images of living cells at 3 days post-NPV-infection. We selected an infected cell whose PIBs filled the whole cell and could be clearly identified by an optical microscope. From its SHG and THG images (Fig. 2), obvious SHG spots were found at the positions where the PIBs were located (Fig. 2(b)). We thus attribute the SHG origin to the PIB crystals. The point-spread-function(PSF)-convoluted apparent sizes of the green spots in this cell range from 1.4 to 2.6 μm. Through optical sectioning of the MV cell at different imaging depth, we could count the total number of the PIBs in this whole cell and the number was 30.
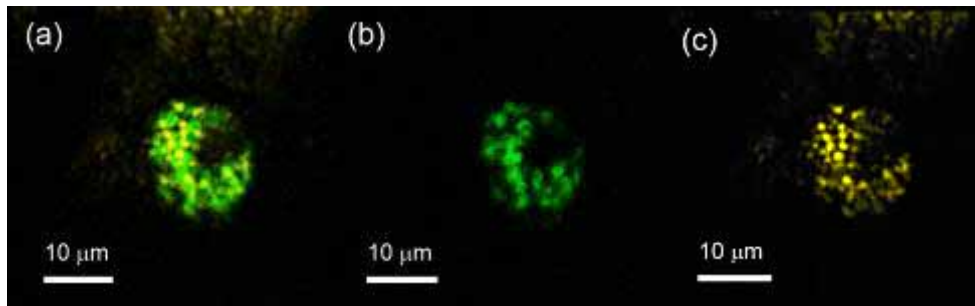

Fig. 2. (a). Combined (b) SHG (green color) and (c) THG (yellow color) image of an infected cell.

We also applied harmonic generation microscopy to other region with living cells, whose PIB crystals were hard to be identified with a traditional microscope, also at 3 days post-NPV-infection. Figure 3 shows a cell with a group of THG signals near the center of the cell, where a virogenic stroma [6], a factory that reproduces virions, can be identified with a traditional microscope. Surrounding the virogenic stroma, there are several SHG spots with PSF-convoluted apparent size ranging from sub-micron to 1.2 μm, which is fewer and smaller than the previous case. There are also THG spots not spatially correlated with SHG signals. They could be the vesicles or the organelles of the cells or the envelope-occluded viruses that had not yet been wrapped in PIB crystals. The identification of the actual THG origin requires further studies and is not within the scope of this current study. With similar procedures, we

checked many other regions of the live cell sample and found that in average one out of ten MV cells had PIB crystals at 3 days post-NPV-infection. The total number of PIB in such a cell was typically 25-30. Compared with a previous work, this value is close to the mean value (~2 PIB/cell) counted by lyzing MV cells [6]. These results indicate that THG of cells have many origins and might cause ambiguity if we use it to identify PIB. In contrast, SHG microscopy is background free for the identification of PIB inside living cells. It provides a more precise way to count the number of PIBs per living cell even in early stages of virus infection.
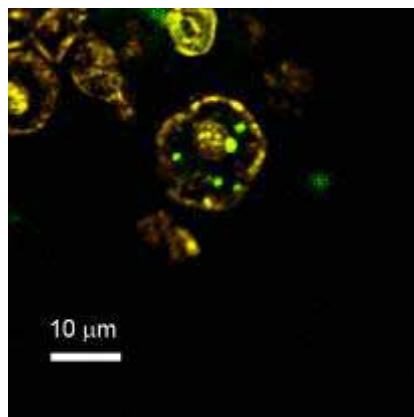

Fig. 3. Combined SHG (green color) and THG (yellow color) image of an infected cell.

4. SHG polarization anisotropy of PIB crystals

To further study if the SHG signals were affected by the protein arrangement in a PIB crystal, we measured the SHG anisotropy of a PIB crystal. We added a half-wave plate right before the scanning unit to rotate the polarization of laser pulses incident on PIBs and simultaneously measured SHG intensities of a single PIB crystal at different SHG polarizations with a SHG-wavelength polarizer in front of the PMT. We set the X-axis as the initial direction of the laser polarization and the Z-axis as the direction of pulse propagation. Since the numerical aperture of the objective is high (NA>0.8), the electric field at the focus will contain Y and Z components [8]. This could affect the modulation depth in SHG anisotropy measurements. However, even for an objective with a 1.4 NA, the power percentage of these tightly-focusing-induced components is only around 10%. In our case with a 0.9 NA objective, this percentage will become even lower and can be treated as a perturbation in the SHG anisotropy analysis [9]. As the polarization of laser pulses rotated counter clockwise around the Z-axis, the measured SHG intensities along the X-axis, I_X, had oscillating periods of 90 degrees (Fig. 4(a), red squares connected with red lines). On the other hand, the measured SHG intensities along the Y-axis, I_Y, also showed two oscillating periods within the 180 degree rotation (Fig. 4(b), red squares connected with red lines). The phase of I_X had a 45 degree offset to that of I_Y. In both traces, the noise background of the SHG signals has been subtracted. Similar results were obtained for other PIBs in the same cell. The angles of peak SHG deviated within 10 degrees.
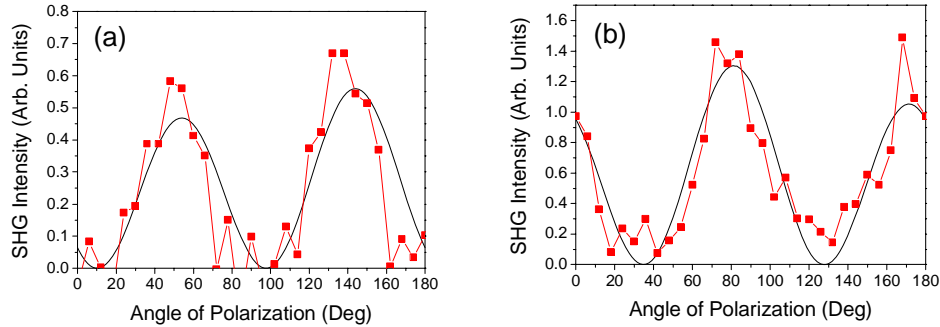
Fig. 4. (a). The SHG intensity along the *X*-axis versus the rotated angle of laser polarization. (b) The SHG intensity along the *Y*-axis versus the rotated angle of laser polarization. Black curves represent the fitting results from the symmetry analysis.

5. Symmetry analysis

The PIB crystal structure of NPV is the same as that of cytoplasmic polyhedrosis virus (CPV) [10]. They are all crystallized from the viral protein, polyhedrin, which has a shape of left hand with thumb (H4) and index finger (H1) outstretched [11]. The H4-helices and the clamp region of three polyhedrins are bundled together, resulting in a trimer with a three-fold symmetry [11]. Rather than an icosahedral shell, these trimers are organized into a body-centered-cubic lattice. To explain how these trimers are arranged in the unit cell of the PIB crystals, we graphically simplify the trimers as a piece of equilateral triangle as illustrated in Fig. 5(a).
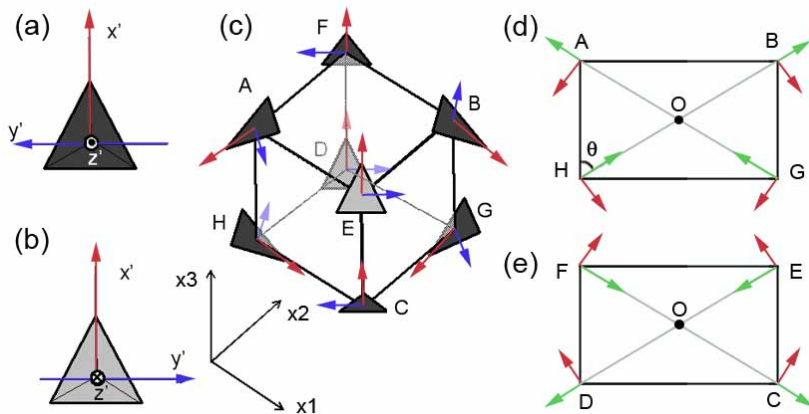

Fig. 5. Coordinate assignment of the simplified trimer with its H4-helices (a) pointing out and (b) into the paper. (c) The arrangement of the trimers in the unit cubic cell of the PIB crystal. Red arrows represent the direction of *x'*-axes and blue the direction of *y'*-axes. The spatial arrangements of trimers in different planes are illustrated: (d) ABGH plane and (e) CDEF plane. Point O is the center of the cubic and green arrows represent the direction of *z'*-axis.

In Fig. 5, the dark gray color represents the side with the H4-helices pointing out of the paper while the light gray color represents the side with the clamp of the trimer (Fig. 5(b)). One apex of the triangle is assigned as the positive direction of the *x'*-axis (Fig. 5, red arrows). The thumbs (H4-helices) point toward the direction of the positive-*z'* (Fig. 5, green arrows). As shown in Fig. 5(c), eight trimers denoted by ABCDEFGH are spatially arranged into a cube. Trimers ABCD have their *z'*-axes pointing outward from the center O of the cube, while the other trimers' have theirs pointing toward it (see Fig. 5(d) and Fig. 5(e)) [11]. Both *x'* and *z'* axes of the trimers ABGH and CDEF lie on the ABGH and CDEF planes, respectively. The

unit cell of the PIB crystal constructed in this way has a body-centered cubic (I23) symmetry [11]. Under such a crystal structure, the effective SHG $\chi^{(2)}$ tensor of the PIB crystal in the *x1-x2-x3* coordinate system (Fig. 5(c)) should consider not only the I23 symmetry but also the local arrangement of the trimers with a three-fold (I3) symmetry. The effective SHG $\chi^{(2)}$ tensor of a local trimer can be expressed as [12]:

$$\overline{\overline{d}}_{tri} = \begin{pmatrix} d_{11} & -d_{11} & 0 & d_{14} & d_{15} & -d_{22} \\ -d_{22} & d_{22} & 0 & d_{15} & -d_{14} & -d_{11} \\ d_{31} & d_{31} & d_{33} & 0 & 0 & 0 \end{pmatrix} . \tag{1}$$

The locally generated SHG polarization $\vec{P}_{loc}(2\omega)$ can be expressed as:

$$\vec{P}_{loc}(2\omega) = \begin{pmatrix} P_{x'}(2\omega) \\ P_{y'}(2\omega) \\ P_{z'}(2\omega) \end{pmatrix} = \overline{\overline{d}}_{tri} \begin{pmatrix} E_{x'}^2 \\ E_{y'}^2 \\ E_{z'}^2 \\ E_{y'}E_{z'} \\ E_{x'}E_{z'} \\ E_{x'}E_{y'} \end{pmatrix}, \tag{2}$$

where $E_{x'}$, $E_{y'}$, and $E_{z'}$ are the field components in the trimer's coordinate. Each component can be further expressed in terms of E_{x1}, E_{x2}, and E_{x3}, which are the field components in the *x1-x2-x3* coordinate. Taking trimer H as an example, its local coordinate can be interpreted by rotating $45°$ around the *x3*-axis and rotating an angle θ around the new *y*-axis, where $\sin\theta = \sqrt{2}/\sqrt{3}$ and $\cos\theta = 1/\sqrt{3}$. The corresponding coordinate transformation is:

$$\begin{pmatrix} E_{x'} \\ E_{y'} \\ E_{z'} \end{pmatrix} = \begin{pmatrix} \dfrac{\sqrt{6}}{6} & \dfrac{\sqrt{6}}{6} & -\dfrac{\sqrt{6}}{3} \\ -\dfrac{\sqrt{2}}{2} & \dfrac{\sqrt{2}}{2} & 0 \\ \dfrac{\sqrt{3}}{3} & \dfrac{\sqrt{3}}{3} & \dfrac{\sqrt{3}}{3} \end{pmatrix} \begin{pmatrix} E_{x1} \\ E_{x2} \\ E_{x3} \end{pmatrix} = T \begin{pmatrix} E_{x1} \\ E_{x2} \\ E_{x3} \end{pmatrix}, \tag{3}$$

and the generated SHG polarization in the PIB's coordinate is $\vec{P}(2\omega) = T^{-1}\vec{P}_{loc}(2\omega)$. Since the size of the cube is much smaller than the optical wavelength, the $\vec{P}(2\omega)$ from each trimer can be directly summed up. Due to a highly symmetric arrangement of these trimers, most terms of the generated SHG polarizations are cancelled by each other and the resulted SHG polarizations along each axis are:

$$P_{x1}(2\omega) = \frac{16}{9}\left(\sqrt{6}d_{11} - 3\sqrt{2}d_{22}\right)E_{x1}E_{x3} + \frac{16\sqrt{3}}{9}(-2d_{15} - d_{31} + d_{33})E_{x2}E_{x3}, \tag{4}$$

$$P_{x2}(2\omega) = \frac{16}{9}\left(\sqrt{6}d_{11} + 3\sqrt{2}d_{22}\right)E_{x2}E_{x3} + \frac{16\sqrt{3}}{9}(-2d_{15} - d_{31} + d_{33})E_{x1}E_{x3}, \tag{5}$$

and

$$P_{x3}(2\omega) = \frac{8}{9}(\sqrt{6}d_{11} - 3\sqrt{2}d_{22})E_{x1}^2 + \frac{8}{9}(\sqrt{6}d_{11} + 3\sqrt{2}d_{22})E_{x2}^2 - \frac{16\sqrt{6}}{9}d_{11}E_{x3}^2 + \frac{16\sqrt{3}}{9}(-2d_{15} - d_{31} + d_{33})E_{x1}E_{x2} . \tag{6}$$

The effective SHG $\chi^{(2)}$ tensor of PIB in the *x1-x2-x3* coordinate system thus becomes

$$\overline{\overline{D}}_{PIB} = \begin{pmatrix} 0 & 0 & 0 & D_{14} & D_{15} & 0 \\ 0 & 0 & 0 & D_{24} & D_{14} & 0 \\ D_{15}/2 & D_{24}/2 & D_{33} & 0 & 0 & D_{14} \end{pmatrix}. \qquad (7)$$

To fit our data with $\overline{\overline{D}}_{PIB}$, the coordinate transformation between the experimental *X-Y-Z* and the PIB's *x1-x2-x3* coordinates should be considered. In our definition, the coordinate transformation from *X-Y-Z* to *x1-x2-x3* can be interpreted by first rotating an angle ϕ around the *Z*-axis, then rotating an angle Θ around the new *x2*-axis, and finally rotating an angle φ around the new *x3*-axis. With this transformation, similar to the procedure of deriving $\overline{\overline{D}}_{PIB}$, the *X* and *Y* components of the generated SHG polarization ($P_X(2\omega)$ and $P_Y(2\omega)$) can also be expressed in terms of the *X* and *Y* components of incident electric field (E_X and E_Y). Because the measured I_X and I_Y are proportional to $|P_X(2\omega)|^2$ and $|P_Y(2\omega)|^2$, we can thus fit them with $\overline{\overline{D}}_{PIB}$ and the parameters used in the coordinate transformation. For the data shown in Fig. 4, thus obtained fitting curve is with $\Theta=100°$, $\phi=30°$, $\varphi=0°$, $D_{14}= -0.2$, $D_{15}=-0.1$, $D_{24}=1.2$, and $D_{33}= -0.5$ (Fig. 4, black curves). That means that the laser beam propagation direction (*Z*-axis) is with a 100° angle from the *x3*-axis of the specific PIB crystal. Because the PIB crystal has an I23 symmetry [11], rotating 180° along the *x1, x2, or x3* axis will result in the same SHG anisotropy. Therefore, the fitting parameters for the SHG anisotropy have a four-fold degeneracy. Since the SHG anisotropy traces can't be fitted by the I23 symmetry, our study indicated that the SHG polarization anisotropy should be induced by the special protein arrangement in a PIB as discussed above. This characteristic polarization anisotropy can be used to identify the presence of PIB crystals from other SHG signal (in case there is any) and the orientation of PIB crystals in images of harmonic generation microscopy [13].

6. Summary

In conclusion, we have demonstrated SHG imaging on PIBs of NPV-infected insect cells. The polarization dependent SHG follows the protein arrangement of the PIB crystal, further validating that the SHG originates from PIB crystals. The size (sub-micron to ~2.6 μm) and the number (25-30) of PIBs in a living cell can thus be studied without lysing cells. This technique can be applied to the 3D evaluation of the yield and the rate of viral infection. It could also be a useful method for studying viral pathology and mass production of insecticide or foreign proteins fused in the PIBs.